



Frictional Behaviour of Masonry Interfaces: Experimental Investigation on Two Dry-Jointed Tuff Blocks

Claudio Intrigila^(✉), Nicola Antonio Nodargi, and Paolo Bisegna

Department of Civil Engineering and Computer Science,
University of Rome Tor Vergata, Rome, Italy
{intrigila,nodargi,bisegna}@ing.uniroma2.it

Abstract. In historical masonry structures, featured by dry or weak mortar joints, limit analysis of 3D assemblages of blocks represents a useful tool for the prediction of failure mechanism and collapse load. Results of limit analysis, with no-tension and frictional contact interfaces, are based on the definition of accurate block interface yield domains: experimental and numerical investigations on the frictional contact conditions are required. Despite the characterization of shear behaviour of frictional contact was widely studied in the past, limited research is available on the behaviour of dry masonry joints implying interactions among shear, bending and torsion. This work aims at presenting an extensive experimental investigation conducted in order to analyse the frictional behaviour of two dry-jointed tuff blocks subjected to loading patterns reproducing several possible yield conditions. Besides providing fundamental parameters required for limit analysis formulations, the adopted testing program investigates 3D yield domains of a single contact interface through different loading scenarios. Moreover, the experimental results are compared with those obtained by a numerical model based on the assumption of rigid blocks which interact through no-tension, frictional interfaces. From the comparison, it is found that the usual modelling hypothesis of ideal interface with all points between blocks perfectly in contact is not always reliable. In fact, depending on the actual contact area and especially in presence of torsion moment, the predicted 3D yield domains may differ significantly from the experimental results.

Keywords: Limit analysis · Experimental interface behaviour · 3D dry-jointed tuff blocks · Shear-torsion-bending interaction

1 Introduction

The structural analysis of historical masonry constructions represents a crucial research topic in the framework of safety and resilience evaluation of artistic and cultural heritage buildings. Ancient structures are generally characterized by an assembly of bricks or stone blocks with interposed weak or dry

mortar joints. Among main approaches presented in the literature aiming at analysing masonry behaviour, it is noteworthy mentioning micro-macro modelling approaches (e.g., see [1–6]), homogenization-multiscale approaches (e.g., see [7–10]) and phenomenological approaches in conjunction with finite element formulations (e.g., see [11–14]).

A different approach is represented by 2D and 3D limit analysis (e.g., see [15–21]) which, simplifying the problem related to the constitutive description of the masonry material with a drastically reduced number of parameters, represents an effective method for the assessment of collapse load and failure mechanism of masonry structures. The appeal of this formulation is the possibility of tracing the analysis back to a linear optimization problem in which the masonry is no longer represented as a continuous material but as an assemblage of rigid blocks, which interact through friction interfaces without tension [17, 18].

In this context, the application of the classical limit analysis theorems, in which the assumption of an associative flow law is correlated to the Coulomb friction governing the behaviour of the interface, leads to a collapse mechanism that shows an interface dilatancy, not evident experimentally. In particular, in order to take into account the lack of dilatancy, the analysis of masonry block structures was gradually formulated as non-associative limit analysis problem in [22–24] and it was subsequently interpreted as a Mathematical Program with Equilibrium Constraints in [25–27]. As a consequence, the loss of uniqueness of the collapse multiplier occurs and the static and kinematic problems are no longer uncoupled.

In this framework, a difficult task is still represented by the definition of interface yield domains in order to adequately describe three-dimensional assemblies of rigid blocks with no mortar. Indeed, the modelling of the actual behaviour of the frictional contact interfaces, with simultaneous shear, torsion and bending is still a novel topic of research [28–31]. Despite the shear behaviour of contact interface was widely studied in the past [32, 33], the lack of experimental data covering various loading scenarios allowed the validation of 3D limit analysis formulations only against results from in-plane loading conditions [34].

General goal of the present work is an experimental investigation on 3D yield domains, with reference to the contact interface between two dry-jointed tuff blocks. By varying the eccentricity of external vertical and horizontal loads, several sets of tests implying interactions among shear, torsion and bending are presented. It should be noted that no standard test procedure is available in the literature. Therefore an ad hoc set-up was designed, as described in the following section.

The experimental results are then compared with those obtained by a standard numerical model proposed in [29, 30], based on the classic assumptions of infinite strength for blocks and frictional no-tension interface behaviour.

The paper is organized as follows. In Sect. 2 the testing procedure is presented and test set-up and testing program are described. In Sect. 3 the experimental results are presented. In Sects. 4 and 5 a comparison with a standard numerical model is reported and discussed. Conclusions are outlined in Sect. 6.

2 Testing Procedure

The test campaign was conducted in the Laboratory of Structures and Material Tests of the Department of Civil Engineering and Computer Science of the University of Rome Tor Vergata. Main goal of the series of experimental tests is the investigation on the 3D frictional behaviour of dry masonry joints. Different cases were carried out on couplet specimens of two dry-jointed Roman yellow volcanic tuff blocks. Typical mechanical characteristics of this tuff were studied in detail in [35]. In order to guarantee the largest possible contact surface of the dry joint, the specimens were previously sawn and rectified by a hydraulic cutting machine. The final dimensions of each block were $300 \times 200 \times 110$ mm ($a \times b \times c$) with a weight of 71 ± 2 N. As depicted in Fig. 1, the lower block was held down by metal devices on a timber board, which was in turn fixed to the testing table. External vertical and horizontal loads were applied to the upper block. Different combinations of axial and shear forces were considered in order to reproduce shear, torsion and bending interaction. To ensure the reproducibility of the tests, at each repetition the interfaces were cleaned of dust by a compressed air machine, as suggested in [30]. Since European standard procedures were not found, the tests were carried out with a specially developed set-up, similar to the one adopted in [30] and described in the next section.

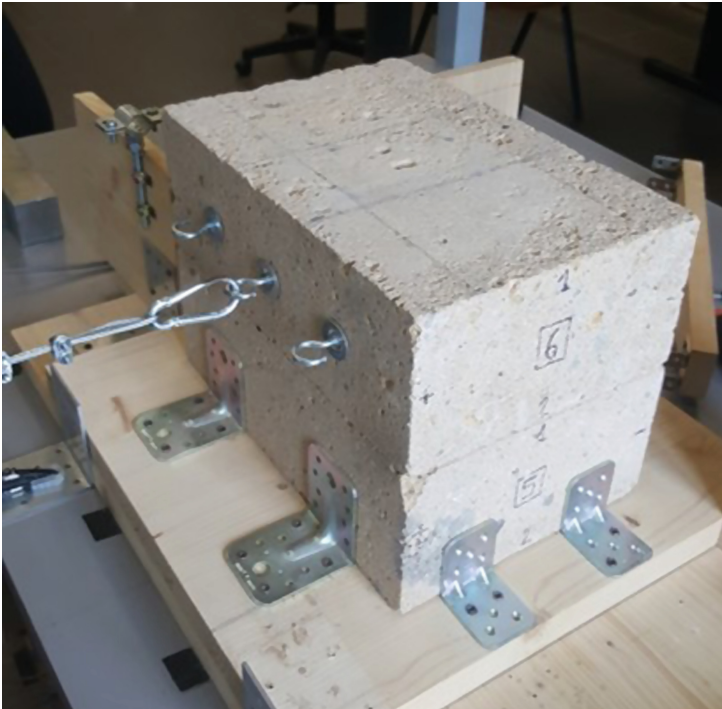


Fig. 1. Specimen of two overlapped tuff blocks.

2.1 Test Set-Up

The experimental tests were carried out using a universal electromechanical testing machine (INSTRON 4482), able to operate under force or displacement control. The two overlapped tuff blocks were placed on an iron table in front of the testing machine. The lower block was fixed to a wooden base by metal brackets, while the upper block was left free, as illustrated in Fig. 2a. A steel cable was connected to the movable crosshead of the testing machine, where a load cell with a maximum load capacity of 10 kN and a sensitivity of 2 mV/V was located. The steel cable, passing through a small pulley, was anchored to the upper tuff block, via steel open-cup-hook bolts located at half of the block height with various eccentricities. The crosshead of the machine was controlled to move up along the vertical direction at a constant displacement rate of 5 mm/min, generating a horizontal force on the upper tuff block, in order to activate the sliding mechanism at the dry joint interface. For the purpose of applying also vertical loads, two steel blocks with dimensions of $300 \times 200 \times 50$ mm and weight of 119 N each, were simply laid on the upper block, with no fixing devices. These plates were placed in different positions in subsequent tests, in order to change the centre of pressure on the interface. Besides the internal displacement transducers of the crosshead, the relative horizontal displacement of the joint was measured by three Linear Variable Displacement Transducers (LVDTs) placed at front, back and lateral sides of the upper tuff block and marked with three different colours (black, red, blue), see Fig. 2b. The adopted LVDTs had a displacement range of ± 25 mm and a linear behaviour range of 0.95% with respect to the maximum displacement. The three independent displacement measures made it possible to identify not only the activation of sliding failure, but also the rigid displacements of the upper block.

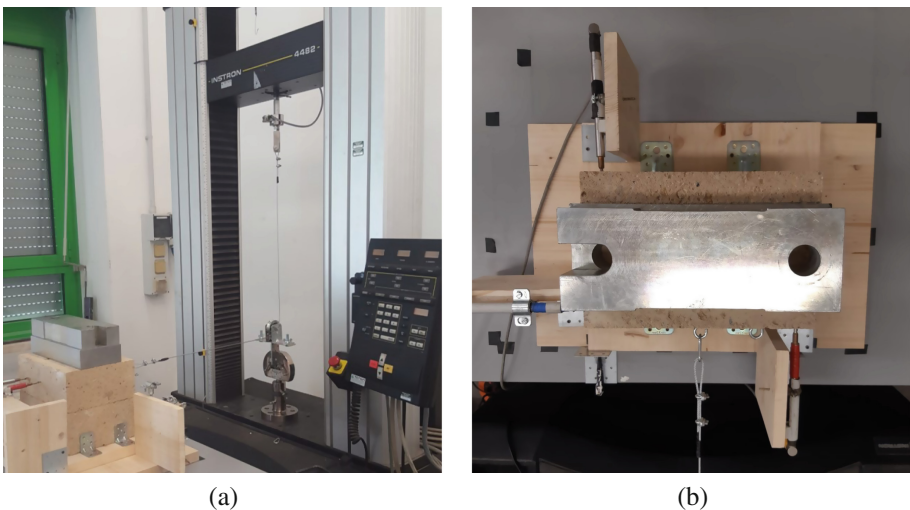


Fig. 2. Test set-up: (a) testing equipment and (b) location of the external LVDTs.

2.2 Testing Program

In the experimental campaign, the influence of the interactions between shear, torsion and bending on the failure behaviour of a single contact interface was investigated. By varying the eccentricity of the vertical and horizontal loads, it was possible to reproduce several possible loading scenarios, providing fundamental results required to validate 3D limit analysis formulations.

Three different testing Sets were considered. All cases of testing Sets are represented in plan view in Fig. 3. In particular, for each case four repetitions were performed. In order to reach a greater accuracy on the value of the friction angle, pure shear series were repeated twice. In Fig. 3, the application point of the resultant of vertical forces on the contact surface is the centre of pressure C . Vertical loads are generated by the overload, given by positioning of the metal plates, and by the weight of the upper block itself.

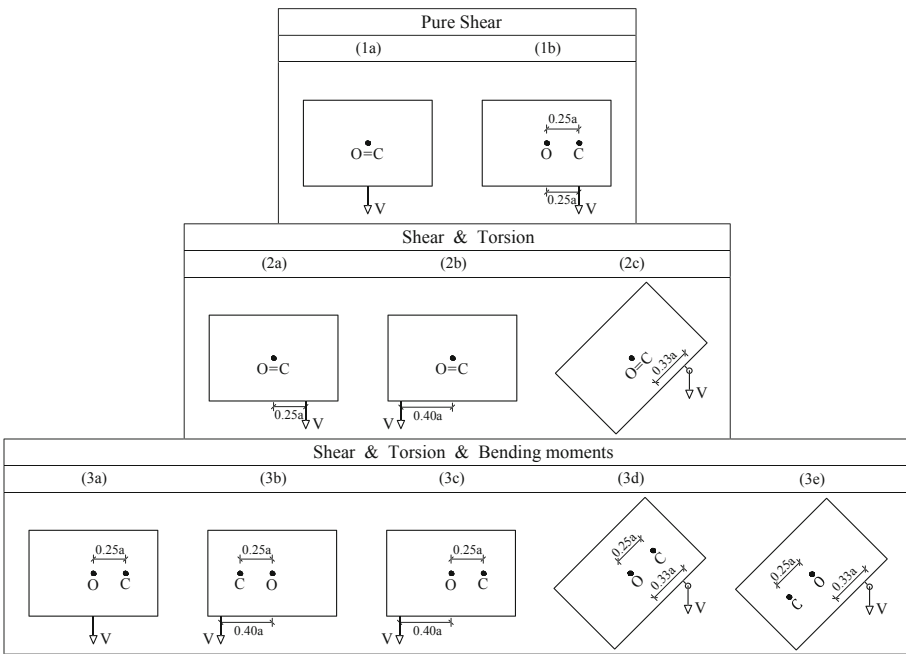


Fig. 3. Testing sets: Pure shear (1a, 1b); Torsion-shear (2a–2c); Torsion-shear-bending (3a–3e).

The pure shear failure was analysed in Sets 1a and 1b. In these cases the line of action of the horizontal force passes through the centre of pressure C , so that no torsion moment arises on the contact interface.

In the second testing Set the interaction among shear and torsion was investigated. In fact, the horizontal force was applied to the upper block with three

different eccentricities (cases 2a–2c) from the centre of pressure, that in turn coincides with the block centre of gravity. Moreover, in case 2c the shear interaction in two direction was developed through the application of the horizontal force inclined by an angle of 45° .

In the third testing Set, through various combinations of application points and orientations of the vertical and horizontal forces, several loading scenarios were analysed for the purpose of investigating the effects of the bending moments on the torsion-shear interaction.

In this study a total of 48 tests were performed.

3 Experimental Results

In this section, experimental results are reported in the same order of the testing program.

3.1 Pure Shear

In this section the results of pure shear tests indicated as Set 1a and 1b are reported and analysed. The Set 1a was carried out by arranging the two steel plates centred on the upper tuff block and by applying, through the pull of the steel cable, the horizontal force at the centre of gravity of the same block, as illustrated in Fig. 4a. Theoretically, in this case, having centred the vertical and horizontal loads, both normal and shear stresses should be uniformly distributed on the contact interface. Although this is not feasible at each point from an experimental point of view [30,36], in the eight tests pertaining this Set the pure sliding behaviour in the horizontal loading direction was observed. Also in the Set 1b no rotation could occur on the joint because the centre of pressure coincides with the point of application of the resultant horizontal force, namely with an eccentricity equal to $0.25a$ (see Figs. 3 and 4b). However, in this case the eccentricity of the centre of pressure and the almost total lack of tensile strength determine a partialization of the contact interface.

The shear force-displacement diagram for case 1b resulting from monotonic test under displacement control is displayed in Fig. 4c. The horizontal load is plotted versus the displacements recorded by the front LVDT (red continuous line) and the back LVDT (black continuous line). Since the transverse displacements of the upper block measured by the lateral blue LVDT were almost negligible, they are not shown in the diagram. A further evidence of the absence of rotation during the test can be detected by the almost coincident aspect of the two curves also in the unloading branches.

These curves show the customary behaviour exhibited in shear load-displacement test, resembling a rigid-plastic behaviour [30,33]. The peak load is rapidly achieved for small displacements and is preceded by a small knee showing non-linear behaviour. After the peak load, a plateau representing an inelastic sliding with a slightly pronounced stick and slip behaviour occurs.

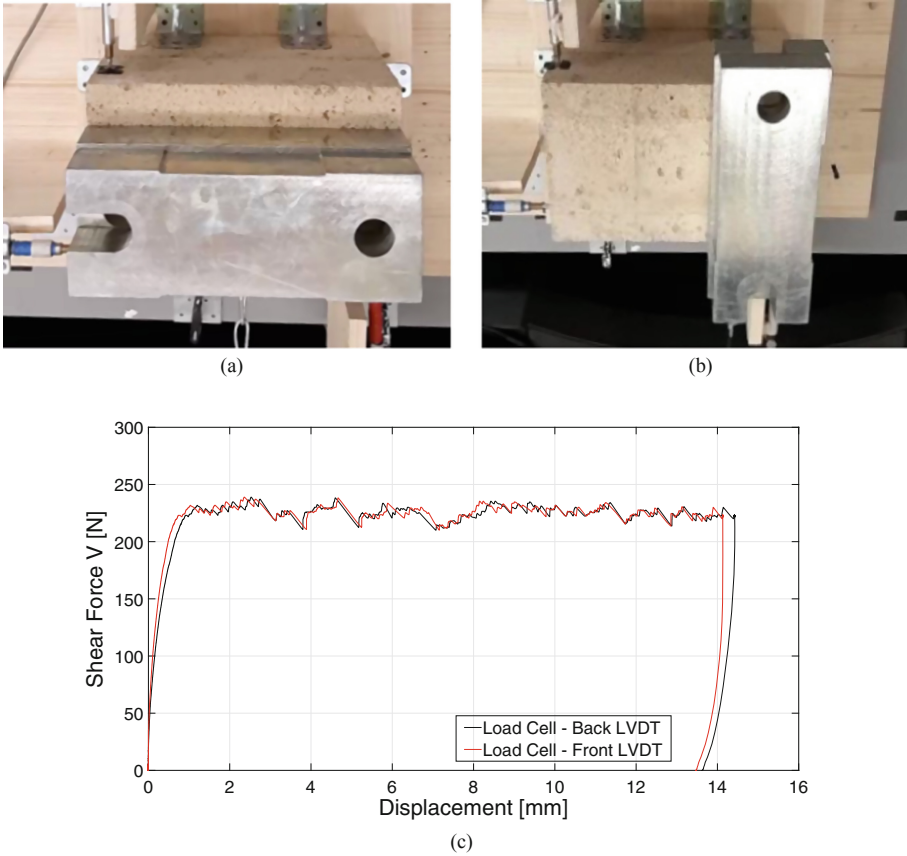


Fig. 4. Pure shear test: (a) Set 1a, (b) Set 1b and (c) Shear force vs displacement curves pertaining to Set 1b (the black curve corresponding to the back LVDT while the red curve corresponding to the front LVDT, see on-line version for coloured figure).

The experimental shear load V activating the sliding failure was obtained by considering a linear fit of the average of the load-displacement curves recorded by the back and front LVDTs at the plateau. The tangent of the friction angle can be represented by the classical Coulomb friction law:

$$\tan \varphi = V/N \tag{1}$$

where N is the resultant of vertical forces on the resistant interface. The value of N is determined by the sum of the applied overload (238 N) on the upper block and the weight of the same block (71 N).

The results of pure shear tests are reported in Table 1. The similarity between the results of successive measurements, that is expressed in terms of standard deviation σ and coefficient of variation σ^* , highlights good accuracy and repeatability of the tests. The value of friction coefficient obtained is $\tan \varphi = 0.72$.

Table 1. Results of testing Sets 1a and 1b

Set	Tests		Statistics			$\tan \varphi$ [-]
	V_{Min} [N]	V_{Max} [N]	V_{Mean} [N]	σ [N]	σ^* [%]	
1a	221.1	226.2	222.9	2.0	0.9	0.72
1b	220.2	223.6	222.0	1.2	0.5	0.72

3.2 Torsion-Shear Interaction

In this section the results of the second testing series are presented. For each Set a sequence of four tests was conducted in order to investigate the interaction among shear and torsion. As shown in Fig. 3, the horizontal force was applied

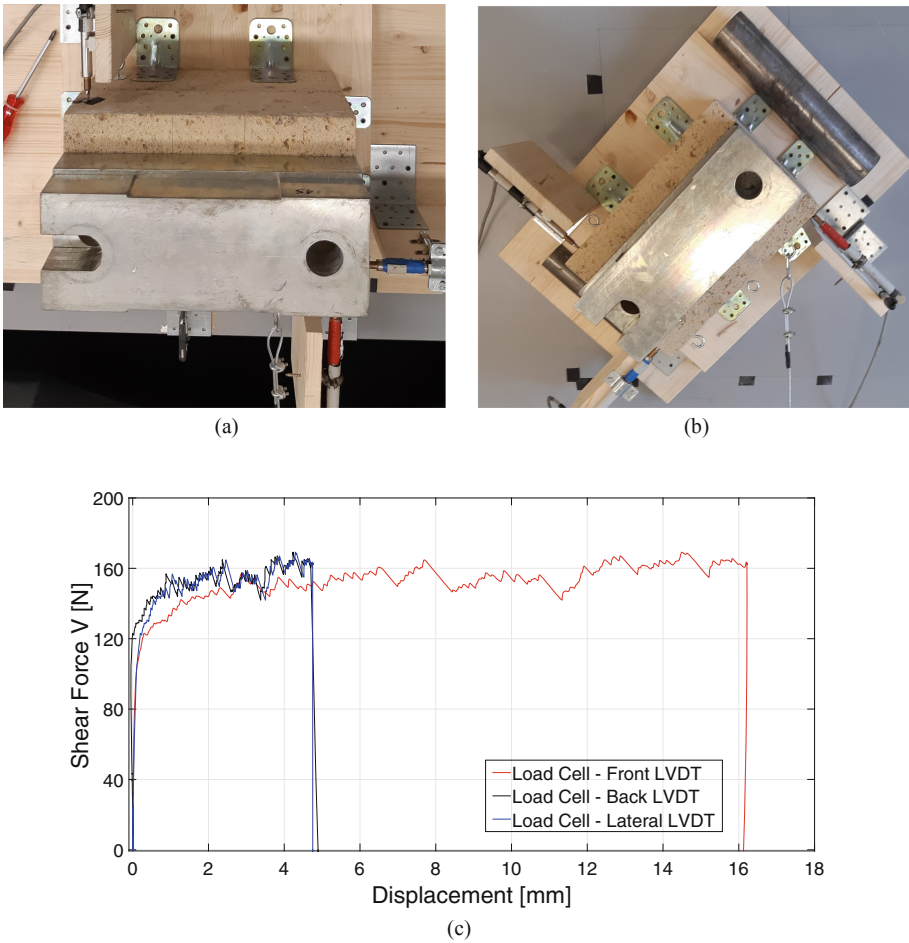


Fig. 5. Torsion-shear tests: (a) Set 2a, (b) Set 2c and (c) Shear force vs displacement diagram pertaining to Set 2a (the black curve corresponding to the back LVDT, the red curve corresponding to the front LVDT and the blue one corresponding to the lateral LVDT, see on-line version for coloured figure).

to the upper block with different eccentricity (cases 2a–2c) from the centre of pressure that coincides with the block centre of gravity. Moreover, in case 2c the shear interaction in two directions was developed through the application of the horizontal force inclined by an angle of 45° , as depicted in Fig. 5b. The three load-displacement curves corresponding respectively to the front (red), back (black) and lateral (blue) LVDTs for Test 1 of Set 2a are plotted in Fig. 5c. The sliding takes place at small displacements but, unlike the previous case of pure shear, the torsion effect determines significantly different displacements recorded by the LVDTs. Indeed, in this case the joint is subjected to a torsion moment and a shear force, therefore the centre of torsion is expected to be located at finite distance from the upper block centre of gravity. In particular, the centre of rotation turns out to be placed at almost the same distance from applications points of the back (black) and lateral (blue) LVDTs and further afar from the front (red) one. This is also consistent with the block kinematics that was video-recorded during the test.

Besides, an apparent hardening branch occurs in the plastic region. As pointed out in [29,30], this effect can be explained by the arising of large displacements. As a matter of fact, after the first noticeable displacement, as the rotation increases, the distance between the application point of the horizontal load and the torsion centre decreases. This means that the horizontal force has to increase to restore the conditions that determined the onset of the mechanism.

For the determination of the shear force value, the red curve representing the front LVDT displacement was considered as the reference curve. In particular, the shear value V was obtained as the y-intercept of the linear regression of the sample data points belonging to the apparent hardening branch. The torsion strength M_T was calculated as the external moment generated by the applied force V with respect to the centre of pressure C and was expressed in absolute value.

In Table 2 the shear values corresponding to the sequence of the four tests conducted for each Set are reported. It can be observed that, as the eccentricity increases, the shear load decreases, as expected.

The variability of the results is higher than in the pure shear case, but still pretty limited, with σ^* values ranging from 3.2% up to 5.2%.

Table 2. Torsion-shear tests: results of series 2a, 2b and 2c. M_T was calculated with respect to the centre of pressure C (see Fig. 3).

Set	Tests				Statistics			M_T [Nm]
	V_1 [N]	V_2 [N]	V_3 [N]	V_4 [N]	V_{Mean} [N]	σ [N]	σ^* [%]	
2a	138.5	140.1	138.9	145.4	140.7	10.6	3.2	2.3
2b	128.7	120.0	116.3	122.4	121.8	14.6	5.2	4.3
2c	95.9	91.4	96.2	85.9	92.3	13.1	4.8	5.2

3.3 Torsion-Shear-Bending Interaction

In this section the results of torsion-shear-bending tests are discussed. As depicted in Fig. 3, by varying the point of application of both horizontal and vertical forces, five different load patterns were experimentally examined.

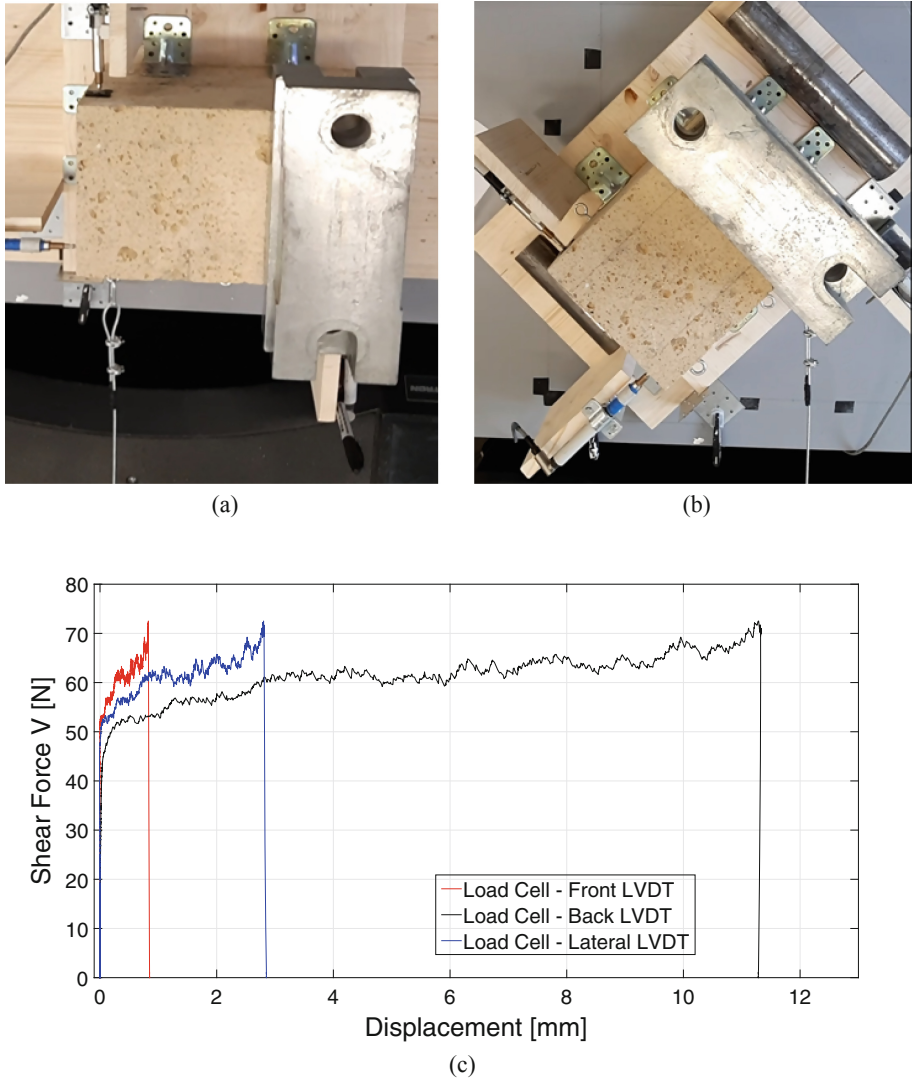


Fig. 6. Torsion-shear-bending tests: (a) Set 3c, (b) Set 3e and (c) Shear force vs displacement curves pertaining to Set 3c (the black curve corresponding to the back LVDT, the red curve corresponding to the front LVDT and the blue one corresponding to the lateral LVDT, see on-line version for coloured figure).

In all the treated cases, for generating the bending moment, the overload was arranged in such a way that its lever arm was equal to $\pm 0.25a$. In the first three testing Sets (3a–3c) the steel cable was positioned orthogonally to the front side of the upper block, while in the other two it was inclined by 45° (3d, 3e). Examples of the arrangement of the loads of these two series are shown in Figs. 6a and b, pertaining respectively to Set 3c and 3e. In Fig. 6c the load-displacement curves for Test 2 of Set 3c are reported. As for torsion-shear interaction case, the large displacement effect after the activation of the mechanism was observed. In this case the displacements registered by the back LVDT were larger than those at the front and lateral ones. This means that the centre of torsion resulted on the opposite side with respect to the horizontal load and, hence, closer to the application point of the front LVDT. This is also highlighted by the low values recorded by the same LVDT.

The experimental results are gathered in Table 3, where V and M_T were still expressed in absolute values, taking into account that M_T was calculated with respect to the centre of pressure C . The results show two fundamental aspects. On the one hand, when the horizontal force was applied in the vicinity of the centre of compression C (Set 3b, 3c), the shear strength was found to approach the pure shear capacity. On the other hand, keeping fixed the centre of pressure C and moving the point of application of the horizontal load to a large eccentricity, a drastic reduction of the shear strength was observed. This trend is in agreement with the experimental results obtained by [29,30].

The variability of the results is enough low, with a σ^* values ranging from 1.3% up to 6.5%.

Table 3. Torsion-shear-bending tests: results of series 3a–3e. M_T was calculated with respect to the centre of pressure C (see Fig. 3).

Set	Tests				Statistics			M_T [Nm]
	V_1 [N]	V_2 [N]	V_3 [N]	V_4 [N]	V_{Mean} [N]	σ [N]	σ^* [%]	
3a	122.1	118.3	120.3	120.2	120.2	1.5	1.3	9.0
3b	175.9	164.3	154.3	153.6	162.0	10.5	6.5	7.3
3c	56.5	55.2	51.1	49.7	53.1	3.3	6.1	10.4
3d	156.5	153.3	142.4	136.3	147.1	9.4	6.4	13.0
3e	49.2	48.4	46.1	45.0	47.2	2.0	4.2	9.2

4 Comparison with Standard Numerical Model

The experimental results presented in Sect. 3 were compared with those obtained from a standard numerical model available in the literature [29,30]. The assumptions of the adopted model are:

- blocks are rigid and interact through Coulomb-frictional interfaces;

- no-tension strength and infinite compressive strength are considered for the frictional contact behaviour;
- failure is concentrated at the centre of the interface, in accordance with the convex contact formulation (e.g., see [31]);
- a uniform distribution of the normal stress is assumed on the resistant contact area.

Under these assumptions, in order to model the contact interface behaviour, the analytical yield domains were derived by [29,30]. The numerical values obtained by “Linear/Linearized” formulation were considered as the reference ones.

All experimental and numerical results in terms of limit shear force are reported in Table 4. For comparison, the relevant σ^* and the relative difference for each case are also reported in Table 4 and displayed in Fig. 7.

The comparison of the linearized numerical model [29,30] against the experimental evidence shows that the predicted yield domains overestimate the interface strength for almost all tests in disadvantage of safety. The highest differences are obtained when a large eccentricity of the horizontal force is considered, e.g. Sets 2c, 3c, 3d. This comparison strongly suggests a poor reliability of the numerical model in the prediction of the tests in which the effects of torsional actions are considerable.

In the other cases, relative differences are approximately less than 20% and in some cases comparable with the relative experimental coefficients of variation σ^* .

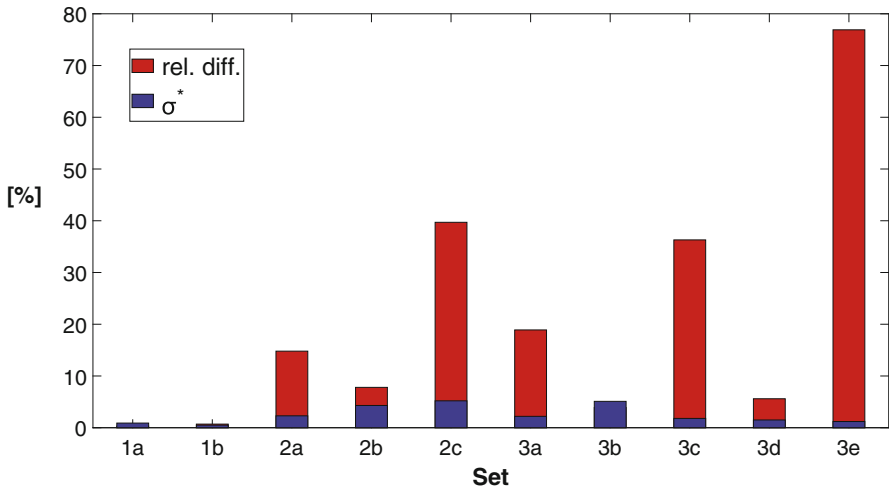


Fig. 7. Comparison between the present experimental results and numerical results obtained by the model in [29,30].

Table 4. Comparison between the present experimental results and numerical results obtained by the model in [29,30].

Set	Experimental		Numerical	Relative difference
	V_{Mean} [N]	σ^* [%]	V_{Mean} [N]	$(Num - Exp)/Exp$ [%]
1a	222.9	0.9	223.6	0.3
1b	222.0	0.5	223.6	0.7
2a	140.7	2.3	161.6	14.8
2b	121.8	4.3	131.2	7.8
2c	92.3	5.2	129.0	39.7
3a	120.2	1.3	142.9	18.9
3b	162.0	6.5	168.4	3.9
3c	53.1	6.1	72.4	36.3
3d	147.1	6.4	155.3	5.6
3e	47.2	4.2	83.5	76.9

5 Discussion

As highlighted in the previous section, the standard numerical model discussed in [29,30] overestimates, in some cases considerably, the experimental results obtained. This could be related to two main aspects. First, the model does not consider the real complexity of the contact interface. Indeed, micro and macro mechanical properties of the tuff joint are just summarized by the friction angle, representing the only input parameter of the model. In particular, to achieve a realistic and reliable simulation of the contact behaviour, the model should take into account the actual lack of homogeneity of the interface, due to possibly nonuniform different roughness distribution of the tuff block faces and

**Fig. 8.** Testing surface: (a) roughness of tested surface and (b) contact surface of the tested specimen

the presence of holes patterns, as depicted in Fig. 8a. Moreover, the numerical model drastically simplifies the resisting contact area, considering the two blocks perfectly in contact at all points of the interface. However, simply inserting a sheet of paper between the two blocks, as illustrated in Fig. 8b, it was possible to verify that the edges of the interfaces were not in contact. This happened especially at the corners of the blocks, that play a significant role in the torsion strength of the interface (as in these areas the shear stresses have larger arms with respect to the centre of pressure).

A proper assessment of the actual contact area can involve variations of the limit torsion strength in the order of 20% and therefore partially justifies the discrepancies between experimental and numerical model results.

6 Conclusions

An experimental investigation on the frictional behaviour of two dry-jointed Roman tuff blocks has been presented. This campaign was carried out in order to investigate the influence of the interaction among shear, torsion and bending on the tuff interface behaviour. Moreover, these experimental results supply fundamental data required for the definition of the interface yield domains that can be employed in the 3D limit analysis formulations.

Since no European standard procedures are available, the test set-up was ad hoc designed on the basis of some recent literature experiments. In the test program, by varying the eccentricities of the horizontal and vertical loads, various possible loading scenarios were analysed.

For each set, the results and the relative variability have been reported. The behaviour of the interface through representative load displacement curves has been described and discussed.

A comparison with results obtained by a standard numerical model based on classical limit analysis assumptions, was performed in terms of limiting shear force. Overall, yield domains predicted by the model overestimate the experimental results, providing in the cases of shear-torsion-bending interaction results even larger than 30%, in disadvantage of safety. It has been observed that these discrepancies could be partly justified by considering the actual contact area. Indeed, through direct inspection, it was verified that the natural irregularities of the blocks had determined the lack of contact in the corner areas. The reduction of these resistant areas has a relevant role on the limit torsion strength of the interface.

Moreover, it is reasonable to think that the friction angle, which often represents the only mechanical parameter of many standard numerical models, may not be sufficient to characterize the actual complicated nature of the masonry stone interface.

A further experimental investigation on blocks with different geometries, i.e. triangular and trapezoidal ones, could provide a useful comparison with the results obtained from this campaign, and an interesting perspective because such stereometry are often present within masonry vaulted structures.

Finally, it is emphasized that the present investigation on the frictional behaviour of dry jointed tuff blocks represents a contribution to the mechanics of masonry block interfaces, a topic which has received little attention in the literature, especially from the experimental point of view.

References

1. Oliveira, D.V., Lourenço, P.B.: Implementation and validation of a constitutive model for the cyclic behaviour of interface elements. *Comput. Struct.* **82**, 1451–1461 (2004)
2. Gambarotta, L., Lagomarsino, S.: Damage models for the seismic response of brick masonry shear walls. Part I: the mortar joint model and its applications. *Earthq. Eng. Struct. Dyn.* **26**, 423–439 (1997)
3. Pelà, L., Cervera, M., Roca, P.: Continuum damage model for orthotropic materials: application to masonry. *Comput. Methods Appl. Mech. Eng.* **200**, 917–930 (2011)
4. Nodargi, N.A., Bisegna, P.: State update algorithm for isotropic elastoplasticity by incremental energy minimization. *Int. J. Numer. Methods Eng.* **105**, 163–196 (2016)
5. Pelà, L., Cervera, M., Roca, P.: An orthotropic damage model for the analysis of masonry structures. *Constr. Build. Mater.* **41**, 957–967 (2013)
6. Nodargi, N.A., Artioli, E., Caselli, F., Bisegna, P.: State update algorithm for associative elastic-plastic pressure-insensitive materials by incremental energy minimization. *Fract. Struct. Integr.* **8**, 111–127 (2014)
7. Milani, G.: Simple homogenization model for the non-linear analysis of in-plane loaded masonry walls. *Comput. Struct.* **89**, 1586–1601 (2011)
8. Petracca, M., Pelà, L., Rossi, R., Oller, S., Camata, G., Spacone, E.: Regularization of first order computational homogenization for multiscale analysis of masonry structures. *Comput. Mech.* **57**, 257–276 (2016)
9. Braides, A., Nodargi, N.A.: Homogenization of cohesive fracture in masonry structures. *Math. Mech. Solids* **25**, 181–200 (2020)
10. Addessi, D., Sacco, E.: A multi-scale enriched model for the analysis of masonry panels. *Int. J. Solids Struct.* **49**, 865–880 (2012)
11. Nodargi, N.A., Caselli, F., Artioli, E., Bisegna, P.: A mixed tetrahedral element with nodal rotations for large-displacement analysis of inelastic structures. *Int. J. Numer. Methods Eng.* **108**, 722–749 (2016)
12. Nodargi, N.A., Bisegna, P.: A novel high-performance mixed membrane finite element for the analysis of inelastic structures. *Comput. Struct.* **182**, 337–353 (2017)
13. Nodargi, N.A.: An overview of mixed finite elements for the analysis of inelastic bidimensional structures. *Arch. Comput. Methods Eng.* **26**, 1117–1151 (2019)
14. Nodargi, N.A., Bisegna, P.: A mixed finite element for the nonlinear analysis of in-plane loaded masonry walls. *Int. J. Numer. Methods Eng.* **120**, 1227–1248 (2019)
15. Kooharian, A.: Limit analysis of voussoir (segmental) and concrete arches. In: *Proceedings of American Concrete Institute*, vol. 89, pp. 317–328 (1952)
16. Heyman, J.: The stone skeleton. *Int. J. Solids Struct.* **2**, 249–279 (1966)
17. Livesley, R.K.: Limit analysis of structures formed from rigid blocks. *Int. J. Numer. Methods Eng.* **12**, 1853–1871 (1978)
18. Livesley, R.K.: A computational model for the limit analysis of three-dimensional masonry structures. *Meccanica* **27**, 161–172 (1992)

19. Como, M.: *Statics of Historic Masonry Constructions*. Springer, Cham (2016)
20. Gilbert, M., Melbourne, C.: Rigid-block analysis of masonry structures. *Struct. Eng.* **72**, 356–361 (1994)
21. Intrigila, C., Nodargi, N.A., Bisegna, P.: Square cross vaults on spreading supports. In: Aguilar, R., Torrealva, D., Moreira, S., Pando, M., Ramos, L.F. (eds.) *Structural Analysis of Historical Constructions*. RILEM Bookseries, vol. 18, pp. 1045–1053 (2019)
22. Fishwick, R.J.: *Limit analysis of rigid block structures*. Ph.D. thesis, Department of Civil Engineering, University of Portsmouth (1996)
23. Baggio, C., Trovalusci, P.: Limit analysis for no-tension and frictional three-dimensional discrete systems. *Mech. Struct. Mach.* **26**, 287–304 (1998)
24. Ferris, M.C., Tin-Loi, F.: Limit analysis of frictional block assemblies as a mathematical program with complementarity constraints. *Int. J. Mech. Sci.* **43**, 209–224 (2001)
25. Orduña, A., Lourenço, P.B.: Three-dimensional limit analysis of rigid blocks assemblages. Part I: torsion failure on frictional interfaces and limit analysis formulation. *Int. J. Solids Struct.* **42**, 5140–5160 (2005)
26. Gilbert, M., Casapulla, C., Ahmed, H.M.: Limit analysis of masonry block structures with non-associative frictional joints using linear programming. *Comput. Struct.* **84**, 873–887 (2006)
27. Nodargi, N.A., Intrigila, C., Bisegna, P.: A variational-based fixed-point algorithm for the limit analysis of dry-masonry block structures with non-associative Coulomb friction. *Int. J. Mech. Sci.* **161–162**, 105078 (2019)
28. Tran-Cao, T.: *Collapse analysis of block structures in frictional contact*. Ph.D. thesis, University of New South Wales, Sydney, Australia (2009)
29. Casapulla, C., Portioli, F.: Experimental and analytical investigation on the frictional contact behavior of 3D masonry block assemblages. *Constr. Build. Mater.* **78**, 126–143 (2015)
30. Casapulla, C., Portioli, F.: Experimental tests on the limit states of dry-jointed tuff blocks. *Mater. Struct.* **49**, 751–767 (2016)
31. Casapulla, C., Maione, A.: Modelling the dry-contact interface of rigid blocks under torsion and combined loadings: concavity vs. convexity formulation. *Int. J. Non-Linear Mech.* **99**, 86–96 (2018)
32. Lourenço, P.B., Ramos, L.F.: Characterization of cyclic behavior of dry masonry joints. *J. Struct. Eng.* **130**, 779–786 (2004)
33. Vasconcelos, G., Lourenço, P.B.: Experimental characterization of stone masonry in shear and compression. *Constr. Build. Mater.* **23**, 3337–3345 (2009)
34. Lourenço, P.B., Oliveira, D.V., Roca, P., Orduña, A.: Dry joint stone masonry walls subjected to in-plane combined loading. *J. Struct. Eng.* **131**, 1665–1673 (2005)
35. De Casa, G., Lombardi, G.: The via Tiberina Yellow Tuff (Rome) used in the Roman monuments. *Rendiconti Lincei. Scienze Fisiche e Naturali* **18**, 5–25 (2007)
36. Jukes, P., Riddington, J.R.: The failure of brick triplet test specimens. *Mason. Int.* **15**, 30–33 (2001)